The Astrophysical Journal, 802:62 (11pp), 2015 March 20 doi:10.1088/0004-637X/802/1/62

X-RAY EVIDENCE FOR A POLE-DOMINATED CORONA ON AB DOR

Jeremy J. Drake[1], Sun Mi Chung[1,2], Vinay L. Kashyap[1], and David Garcia-Alvarez[1,3,4]
[1] Smithsonian Astrophysical Observatory, MS-3, 60 Garden Street, Cambridge, MA 02138, USA; jdrake@cfa.harvard.edu, vkashyap@cfa.harvard.edu
[2] Department of Astronomy, The Ohio State University, 4055 McPherson Laboratory, 140 West 18th Avenue, Columbus, OH 43210-1173, USA; chung@astronomy.ohio-state.edu
[3] Instituto de Astrofísica de Canarias, E-38205 La Laguna, Tenerife, Spain; david.garcia@gtc.iac.es
[4] Departamento de Astrofísica, Universidad de La Laguna, E-38206 La Laguna, Tenerife, Spain
Received 2014 November 10; accepted 2015 January 23; published 2015 March 23

ABSTRACT

A fine analysis of spectral line widths and Doppler shifts employing Fourier transform and cross-correlation techniques has been applied to *Chandra* HETG spectra obtained in 1999 October of the rapidly rotating young star AB Doradus in order to investigate its coronal topology. The observation lasted 52.3 ks, covering 1.2 rotation periods. The X-ray light curve obtained from integrating the dispersed signal revealed a moderate intensity flare midway through the exposure in which the count rate increased sharply by about 50% and subsequently decayed over the next 10 ks. We find no significant Doppler shifts in the spectra or modulation of the light curve that could be attributed to rotation of dominant coronal structures at this epoch. Individual spectral line widths are statistically consistent with thermal broadening and formally require no rotational broadening, while the 1σ limit to rotational broadening corresponds to a compact corona restricted to latitudes $<57^\circ$. Fourier analysis suggests a small amount of rotational broadening is present consistent with a corona restricted largely to the poles, and excludes models with surface rotational broadening or greater. These results present direct spectroscopic evidence that the dominant coronal activity on rapidly rotating active stars is associated with the dark polar spots commonly seen in photospheric Doppler images and support models in which these spots are of mixed magnetic polarity that forms closed loops.

Key words: stars: coronae – stars: late-type – stars: magnetic field – stars: rotation – stars: winds, outflows – X-rays: stars

1. INTRODUCTION

The Sun is the only star for which we can presently image coronal X-ray emission directly. In order to understand how coronae on other stars might be structured we must resort to indirect means, such as eclipse or rotational modulation, and spectroscopic density diagnostics. The advent of the "high resolution" ($\lambda/\Delta\lambda \sim 1000$) capability of the X-ray transmission grating spectrometers on the *Chandra* X-ray Observatory opened up further possible means of probing coronal structure. One of these is through the Doppler shifts of spectral lines in the X-ray-emitting plasma that arise as a result of orbital or rotational motion.

For late-type stars, the velocities involved are typically of order 10–100 km s^{-1}—easily sufficient for optical studies of rotationally driven changes in spectral line profiles that are now routinely "inverted" to make quite detailed Doppler images of surface features of varying brightness (see, e.g., Strassmeier 2002) and Zeeman Doppler images of surface magnetic features (e.g., Donati & Landstreet 2009). However, for instruments with a resolving power of ~1000, such velocities only amount to a fraction of the instrumental width, and Doppler studies are challenging. Nevertheless, several studies have now demonstrated the utility of *Chandra* LETG, HETG spectra for probing both orbital velocities, and rotationally modulated Doppler shifts in magnetically active stellar systems, both binaries (e.g., Brickhouse et al. 2001; Ayres et al. 2001; Chung et al. 2004; Huenemoerder et al. 2006; Ishibashi et al. 2006; Hussain et al. 2012), and single stars (e.g., Hussain et al. 2005; Drake et al. 2008).

In addition to detecting Doppler shifts in the *Chandra* HETG spectrum of Algol caused by the orbital motion of Algol B, Chung et al. (2004) also found spectral line widths to have excess line broadening amounting to approximately 150 km s^{-1} above that expected from thermal motion and surface rotation. The excess broadening implied that a significant component of the corona at temperatures less than 10^7 K has a scale height of order the stellar radius. A similar line width analysis applied to the rapidly rotating giant FK Com by Drake et al. (2008) revealed Doppler shifts consistent with localized emission on one hemisphere with a scale height of about a stellar radius.

The young K-type dwarf AB Doradus, with a projected rotational velocity of 90–100 km s^{-1} (Rucinski 1985; Vilhu et al. 1987; Donati & Collier Cameron 1997), presents a plausible, though challenging, case for Doppler inference of coronal structure based on *Chandra* spectra. Hussain et al. (2005) found evidence for rotational Doppler shifts in *Chandra* LETG spectra, while Hussain et al. (2007) combined *Chandra* data with Zeeman Doppler imaging (ZDI) of the stellar surface to infer coronal structure and scale height. Cohen et al. (2010) have also employed ZDI maps in order to infer coronal structure based on detailed magnetohydrodynamic (MHD) corona and wind models.

Here, we bring further, potentially more sensitive, analysis techniques to bear on the *Chandra* HETG spectra of AB Dor. The analysis partly follows methods developed in the study of Algol HETG spectra by Chung et al. (2004), to which the reader is referred for a more detailed technical discussion. We use cross-correlation and Fourier techniques to to determine where the bulk of the observed X-ray emission originates in this system at this epoch. AB Dor is introduced in the light of

existing work in Section 2, and the *Chandra* observations and analysis are described in Section 3. The results of the analysis are discussed in Section 4 before drawing the main conclusions from the study in Section 5.

2. AB DOR AND ITS CORONAL ACTIVITY

AB Doradus (HD 36705) is a relatively bright ($V = 6.9$), rapidly rotating K0 star at a distance of about 15 pc, with a period $P = 0.514$ days (Pakull 1981). Its mass is estimated to be $0.86M_{\odot}$ and it is in orbit with a distant companion of mass $0.09M_{\odot}$ (Guirado et al. 1997, 2010). Based on the similarity of its space velocity with that of the Pleiades moving group (Innis et al. 1985), and short period and high Li abundance (Rucinski 1985; Vilhu et al. 1987), AB Dor was commonly accepted as a young star coeval with the stars of the Pleiades (~100 Myr) and that is just evolving onto the main sequence. However, the exact age of AB Dor has been a topic of continuing controversy, with estimates ranging from as young as 30 Myr to as old as 125 Myr (e.g., Collier Cameron & Foing 1997; Zuckerman et al. 2004; Luhman et al. 2005; Janson et al. 2007; Torres et al. 2008; da Silva et al. 2009; Guirado et al. 2011; Barenfeld et al. 2013; McCarthy & Wilhelm 2014; Wolter et al. 2014). The preponderance of these studies favor an age of at least 100 Myr or so.

The radius of AB Dor was recently measured to be $0.96 \pm 0.06R_{\odot}$ based on near-infrared interferometry (Guirado et al. 2011). Commensurate with youth, rotational modulation of the photometric light curve of AB Dor, as well as extensive optical Doppler imaging studies, suggest that its surface is covered with large, cool starspots or "maculae," switching between active longitudes on a 5.5 yr cycle and probably modulated with a cyclic period of about 20 yr (e.g., Rucinski 1985; Vilhu et al. 1993; Donati et al. 1999; Järvinen et al. 2005; Budding et al. 2009; Arzoumanian et al. 2011 and references therein). The detailed distribution of these spots has been studied in surface brightness maps obtained over many years. They show a persistent polar cap, together with variable mid to low-latitude spots (e.g., Donati & Collier Cameron 1997; Jeffers et al. 2007). The related technique of ZDI has been extensively employed on AB Dor to study its surface magnetic field distribution and evolution. The magnetic field maps reveal strong, complex field distributions. Donati et al. (1999) reported at least 12 different radial field regions of opposite polarities located all around the star from observations obtained in 1996 December. They found a degree of five or greater for a spherical harmonics expansion of the underlying large-scale poloidal structure. There is also a strong and often unidirectional azimuthal field encircling the boundary of the polar cap found in the spot maps.

There are several existing photometric and spectroscopic observational clues as to the structure of the corona of AB Dor. Rotational modulation studies based on EUV-X-ray observations of coronal emission can, in principle, render some limited spatial information. Evidence for such modulation has been only very marginal in GINGA and *EXOSAT* observations (Collier Cameron et al. 1988; Vilhu et al. 1993), and essentially absent in *Extreme-Ultraviolet Explorer* and ASCA data (White et al. 1996). A lack of strong rotational modulation implies either one or more of the following: emission is distributed fairly uniformly in azimuth; emission is extended with a scale height of order the stellar radius or larger; emission is concentrated at the stellar poles. Later extensive monitoring with *ROSAT* revealed modest ~5–13% modulation in pointed observations and 19% modulation in all-sky survey data (Kuerster et al. 1997), indicating the presence of some lower-latitude structure non-uniform in stellar longitude. Maggio et al. (2000) reported an observation of a compact flare (height $\lesssim 0.3R_{\star}$), which took a rotation period to decay and showed no evidence of self-eclipse, indicating a high-latitude location. At lower chromospheric and transition region temperatures ($\sim 10^4$ -10^5 K), rotational modulation was seen in the fluxes of FUV lines (Schmitt et al. 1997; Ake et al. 2000). More recently, Lalitha & Schmitt (2013) did not find evidence for persistent rotational modulation based on *XMM-Newton* observations obtained over the past decade and attributed observed variability to stochastic processes such as flares.

Perhaps more interesting are spectroscopic constraints. García-Alvarez et al. (2005) found the coronal spectrum essentially identical to that of the Hyades tidally locked close K1 V+DA binary V471 Tau that has been spun up to a very similar rotation period. Both spectra exhibit a fairly broad range of coronal temperatures up to 10^7 K or so, and coronal abundances that deviate from the solar mixture in according to an "inverse First Ionization Potential" effect pattern that is typical of active stars (see, e.g., Brinkman et al. 2001; Drake et al. 2001; Drake 2003). Sanz-Forcada et al. (2003b) deduced a coronal scale height of less than the stellar radius based on electron densities estimated from *XMM-Newton* spectra, similar to density and optical depth constraints on scale height for other active stars (Sanz-Forcada et al. 2003a; Ness et al. 2004; Testa et al. 2004a, 2004b, 2007).

Hussain et al. (2005) found evidence for rotational Doppler shifts in lines of O VIII observed using the *Chandra* LETGS in 2000 December, suggesting the presence of low-latitude compact emitting regions. Analysis of HETGS Fe XVII λ15.01 and FUSE Fe XVIII λ974 line profiles indicated a coronal scale height of $\lesssim 0.5$ $R_{\star}$. Hussain et al. (2007) combined the *Chandra* observations with ZDI reconstructions of the surface magnetic field and its extrapolation into the corona, and concluded that coronal structures are no more than $0.3–0.4R_{\star}$ in height. Cohen et al. (2010) used a ZDI surface magnetic map based on spectropolarimetric observations obtained in 2007 December to drive a global MHD model of the wind and corona of AB Dor. They found the global structure of the stellar corona at lower latitudes was dominated by strong azimuthal wrapping of the magnetic field due to the rapid rotation. Lalitha et al. (2013) obtained simultaneous radio, optical, and X-ray observations covering a multi-component flare and found flaring filling factors of 1% –3% of the stellar surface.

At cooler temperatures, rotational broadening has been detected in lines of both C III (λ977, λ1175) and O VI (λ1032, λ1037) in ORFEUS and FUSE spectra (Schmitt et al. 1997; Ake et al. 2000). Schmitt et al. (1997) note that this does not exceed the photospheric $v \sin i$ value, suggesting that the observed C III and O VI emission is produced close to the stellar surface. Based on later FUSE spectra obtained in 2003 December, Dupree et al. (2006) infer activity at mid-latitudes with a scale height of $\sim 1.3–1.4R_{\star}$. Optical spectroscopy has also revealed the presence of prominences, initially through discrete absorption features in Hα (Robinson & Collier Cameron 1986; Collier Cameron & Robinson 1989), and subsequently also in the light of Mg II and Ca II (Collier Cameron et al. 1990). These prominences comprise cool (8–10,000 K) clouds of neutral, or near neutral, hydrogen at,

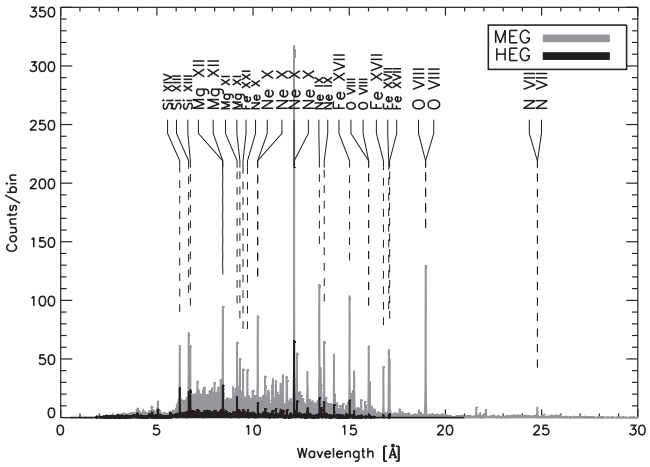

Figure 1. The *Chandra* HETG spectrum of AB Dor, for both HEG and MEG binned at 0.0025 and 0.005 Å intervals, respectively. Emission lines that were used in our analyses are labeled in a larger font size than lines that were not used.

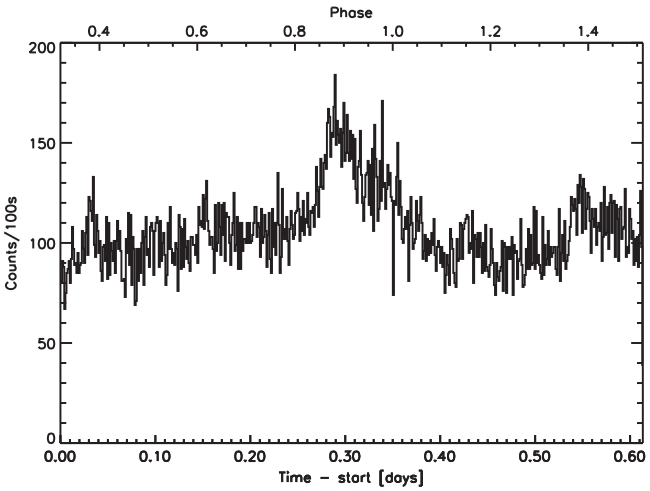

Figure 2. The observed X-ray light curve of AB Dor derived from dispersed HEG and MEG events, plotted as a function of rotational phase. The top axis shows the rotational phase computed with the ephemeris of Innis et al. (1988), and the bottom axis shows the elapsed time in days since the start of the observation.

and also perhaps beyond, the Keplerian co-rotation radius. Collier Cameron et al. (1990) estimated that between 5 and 20 prominences were present in 1988 December, each with a mass of a few 10^{17} g. Ultraviolet spectroscopy with the *HST* Goddard High Resolution Spectrograph revealed narrow chromospheric line cores superimposed on very broad line wings, the latter being consistent with a location commensurate of that of the optically detected prominences (Brandt et al. 2001). Analogous structures have also been detected in the K dwarf component of V471 Tau based on C II and C IV absorption in FUSE spectra by Walter (2004). Young G and K dwarfs of the α Persei cluster also show evidence of the same behavior, indicating that such prominences are likely a common feature of rapidly rotating stars (Collier Cameron & Woods 1992).

All these observations provide a rather complex, and sometimes inconsistent, picture of the corona of AB Dor. In the following sections we examine the only existing *Chandra* HETG spectrum of AB Dor, and the highest resolution X-ray spectrum of the star obtained to date that presents lines bright enough for detailed study, for further clues as to its outer atmospheric structure.

3. OBSERVATIONS AND ANALYSIS

AB Dor was observed using the *Chandra* HETG and ACIS-S detector on 1999 October 9 11:21 UT for a total net exposure of 52.3 ks, or approximately 1.2 stellar rotation periods. The data analyzed here were obtained from the *Chandra* public archive.[5] The final extracted spectrum showing the spectral lines used in this analysis is illustrated in Figure 1. Our analysis methods described below, involving light curves, cross-correlation techniques and line profile modeling, are similar to those described by Chung et al. (2004) and Drake et al. (2008), to which the reader seeking more detail is referred.

3.1. Light Curve

Prior to performing detailed spectral analysis, the *dispersed* photon events were first examined to ascertain the level at which AB Dor varied in X-rays during the observation. Owing to the ACIS-S 3.2 s frame time, zeroth-order events are significantly affected by photon pile-up and do not yield accurate photometry and are ignored here. Flares and rotational modulation caused by dominant active regions are of particular interest since the location of their X-ray source might be betrayed by rotationally induced Doppler shifts, providing direct observational clues as to the locations of coronal activity.

The X-ray light curve obtained from both HEG and MEG dispersed events binned at 100 s intervals is illustrated in Figure 2. We also show in this figure the rotational "phase" computed according to the ephemeris of Innis et al. (1988), HJD = 2444296.575+0.51479E. There are several very small flare-like brightenings visible, but the light curve is dominated by a moderate flare occurring midway through the observation. There is no obvious impulsive phase and the apparent flare rise time is of order 2000 s, which might be considered long for a flare of this size whose decay timescale is of order 10,000 s. It is possible that an impulsive phase was occulted by the stellar disk just prior to rotating into view, though Doppler shift measurements discussed below suggest this might not be the case.

While the light curve does not appear to show any structure that might be commensurate with rotational modulation, the relatively short duration of the observation covering only slightly more than a single phase, combined with the flare, does hinder our ability to detect such modulation if it were present. The flatness of light curve outside of the large and smaller flares indicates that the amplitude of any rotational modulation can only be of the order of 10% or less.

3.2. Phase-related Doppler Shifts

As noted above, Doppler shifts of spectral lines as a function of time might betray the presence of particularly dominant coronal structures. The equatorial velocity of AB Dor is about 95 km s^{-1}, which amounts to approximately 25% of the width of the O VIII 18.97 Å Ly$_\alpha$ doublet as seen by the MEG; such a

[5] http://asc.harvard.edu/cda

Table 1
A List of Emission Lines Used in Our Analyses, Including the Rest Wavelength, Element and Ion, and Grating

Wvl [Å]	Ion	Grating	Analysis
8.42	Mg XII	MEG,HEG	Doppler Shifts
12.13	Ne X	MEG,HEG	Both
14.20	Fe XVIII	MEG	Both
15.01	Fe XVII	MEG,HEG	Both
16.01	O VIII	MEG	Both
16.78	Fe XVII	MEG	Both
18.97	O VIII	MEG	Both
24.78	N VII	MEG	Both

Note. The last column indicates whether the lines were used in Doppler shift or line broadening analyses.

shift should be easily detectable in the brighter spectral lines of the AB Dor soft X-ray spectrum.

3.2.1. Analysis of Individual Spectral Lines

In the first part of our analysis we searched for Doppler shifts of individual spectral lines as a function of time. Lines used in this analysis are listed in Table 1. These represent the strongest lines in the HETG spectrum of AB Dor longward of 8 Å. While H-like and He-like lines of Si are also reasonably bright, the resolving power of the *Chandra* gratings is generally too low at these wavelengths to be of significant additional value in this line-by-line part of the study.

Dispersed events within wavelength ranges of interest for our chosen lines were binned over different time intervals, depending on the number of counts in each line, so as to achieve approximately the same signal-to-noise ratio in each bin. Positive and negative orders were co-added, then analyzed. Line wavelengths were measured by fitting modified Lorentzian functions ("β-profiles") described by the relation

$$F(\lambda) = a/\left(1 + \left(\frac{\lambda - \lambda_0}{\Gamma}\right)^2\right)^{\beta}, \quad (1)$$

where a is the amplitude and Γ is a characteristic line width. For a value of the denominator exponent $\beta = 2.5$, this function has been found to be a good match to observed HETGS line profiles, which are not well-matched by Gaussian profiles (Drake 2004). Fitting was performed using the *Package for INTerative Analysis of Line Emission* (*PINTofALE*[6]; Kashyap & Drake 2000) IDL[7] software routine FITLINES. Uncertainties at the 1σ level were determined from a thorough search of the goodness-of-fit surface.

Since the HETG observation covered slightly more than one full rotation period, we determined line positions in the individual time-filtered bins relative to the wavelengths measured for the same lines from the entire observation. In this way, we avoid complications from small wavelength calibration errors or any long-term drift in the dispersion relation. The measured relative line positions as a function of time are illustrated in Figure 3. The resulting line positions are fairly stable with little change as a function of orbital phase. There is a suggestion of a redshift at phase $\phi \sim 0.9$ in Fe XVII λ16.78 and Mg XII λ8.42, but this signature is not seen in other lines. The O VIII λ18.96 line also shows some evidence for a secular trend with a single point near $\phi \sim 0.8$ exhibiting a 2σ variation from the zero level, but this trend is opposite that which one might be tempted to see in O VIII λ16.01; the latter is actually perfectly consistent with a zero net velocity shift.

3.2.2. Cross-correlation Analysis

In addition to measuring individual emission lines, we also utilized a cross-correlation technique to obtain Doppler shifts as a function of rotational phase. The method involves comparison of the spectra extracted for the different time bins with a reference spectrum in order to determine whether or not there is a net Doppler shift between the two. This technique was first developed during earlier analyses of *Chandra* HETGS observations of Algol (Chung et al. 2004) and FK Com (Drake et al. 2008), and we refer the reader to those works for a more detailed description. The advantage of this type of cross-correlation technique over the analysis of individual spectral lines is that it utilizes the signal from the whole spectrum—strong and weaker lines, isolated and blended—and is therefore, at least in principle, much more sensitive. There are about 12 strong lines longward of 10 Å in the MEG that have the highest velocity sensitivity and will provide the greater part of the signal, and a similar number in the HEG spectrum, although, again, all features in the spectrum contribute. The disadvantage of the technique is that it potentially confuses structures with different characteristic temperatures since it uses lines formed over a fairly large temperature interval. We return to this in Section 4.1.

Events were binned into five time intervals corresponding to different rotational phases, and spectra were extracted for each phase bin. These spectra were then cross-correlated with the reference spectrum, which in this case was the spectrum extracted from the entire exposure, in order to determine the velocity shift at which our correlation signal (represented by a χ^2 statistic) was minimized. As in the analysis of Algol, the uncertainties in this procedure were estimated using a Monte Carlo technique in which the analysis was repeated a number of times for different Poisson realizations of the spectra. The analysis was undertaken for both the HEG and MEG spectra separately. The full range of each spectrum that contained significant signal was used. These ranges were 2–26 Å and 2–18 Å for MEG and HEG, respectively.

Figure 4 illustrates the line-of-sight velocity of AB Dor as a function of rotational phase obtained from the cross-correlation method, for the MEG (upper) and HEG (lower) data. There are clearly no large velocity shifts detected, with the more sensitive, by virtue of the number of photon counts, MEG data placing quite stringent limits on average net velocity excursions of less than about 20 km s^{-1}. In the context of the projected surface equatorial rotational velocity of 95 km s^{-1}, this lack of obvious systematic Doppler shifts indicates that the corona of AB Dor is not dominated by one or two low-latitude active regions; the X-ray emission must be more evenly distributed over the surface, or else resides predominantly toward polar regions for which projected rotation velocities are small.

3.3. Spectral Line Widths

The two scenarios mentioned above can in principle be diagnosed by examining spectral line widths to search for

[6] PINTofALE is publicly available at http://hea-www.harvard.edu/PINTofALE/.
[7] Interactive Data Language, Exelis Inc.

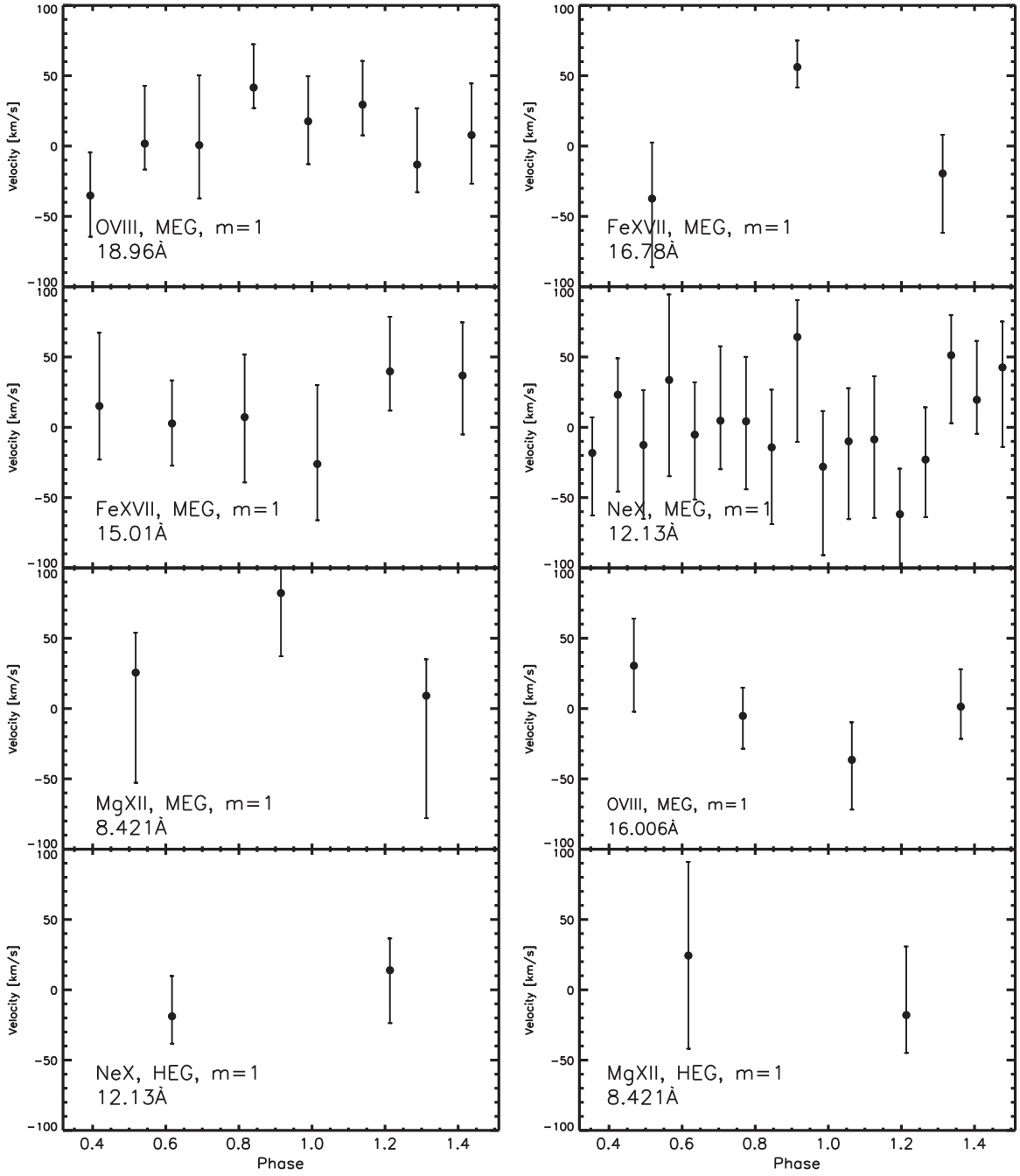

Figure 3. The observed line-of-sight orbital velocity and 1σ error bars as a function of rotational phase for lines listed in Table 1, expressed relative to the measured wavelength for the entire observation.

excess rotation-related broadening. In our analysis, we compared line widths of observed data to those of model profiles, which include the effects of thermal, rotational, and instrumental broadening. The procedure was again developed from that originally discussed in detail by Chung et al. (2004) and Drake et al. (2008).

In order to minimize uncertainties in the calibration of the instrument line response function, we carried out the AB Dor line width analysis relative to an evolved star μ Vel, which is known to have a very small projected rotation velocity of $v \sin i = 6\ \mathrm{km\ s^{-1}}$ (de Medeiros & Mayor 1995). Synthetic line profiles were calculated for μ Vel based on the DEM obtained from the *Chandra* HETG spectrum by García-Alvarez et al. (2006).

Lines used in this analysis are listed in Table 1. The Mg XII λ8.42 line was excluded in the line width analysis because the dispersion at this wavelength is insufficient to clearly discriminate between line widths of theoretical profiles with no rotational broadening versus those broadened by surface rotation. Theoretical line profiles were synthesized by convolving the thermal, rotational, and instrumental line broadening components. Details of theoretical line synthesis may be found in Chung et al. (2004). Thermal broadening was computed using the differential emission measure as a function of

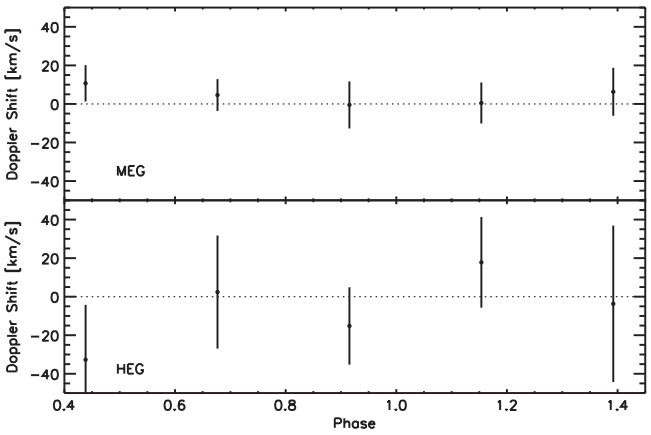

Figure 4. The line-of-sight velocity as a function of rotational phase for MEG and HEG spectra, obtained by cross-correlating spectra from different time intervals with the spectrum from the entire observation.

temperature, $\Phi(T)$, derived from the same HETG spectra by García-Alvarez et al. (2005). For rotational broadening we assumed solid body rotation of the stellar surface (e.g., Gray 1992), corresponding to the projected rotational velocity $v \sin i = 95$ km s^{-1}. The stellar radius, $R_\star$, was taken to be $1R_\odot$, which is consistent with the interferometric result $0.96 \pm 0.06R_\odot$ of Guirado et al. (2011). We also synthesized profiles for different effective radii to simulate the effects of rotation of a corona with a scale height significantly above the stellar surface.

Observed line widths were measured as described in Section 3.2.1. Table 2 lists the line widths of AB Dor and μ Vel for observed and model profiles, together with the AB Dor excess widths relative to μ Vel. We also illustrate the AB Dor excess line widths in Figure 5. The uncertainties for these excess line widths relative to μ Vel correspond to the quadrature propagation of the uncertainties of the individual AB Dor and μ Vel line widths. Also shown are the theoretical line widths corresponding to the case of no rotation, rotation at the stellar surface, and rotation at one stellar radius above the stellar surface, all relative to μ Vel. Here, we define the scale height as the height above the stellar surface. Note that, under this definition, negative scale heights are possible and correspond to the case where rotational broadening is less than that induced by rotation of uniform surface emission.

In most cases the observed line widths in Figure 5 are consistent with the theoretical profiles corresponding to zero rotation, within observational errors. Most of the lines are also consistent, within errors, with theoretical profiles that include rotational broadening at the stellar surface. In order to determine to what extent the observations of individual lines can constrain the scale height of the emission of AB Dor, we combined the individual results in the following way. For each AB Dor line width we subtracted the appropriate μ Vel line width, then generated 100 Monte Carlo realizations within a normal distribution corresponding to the observed AB Dor line width (relative to μ Vel) and 1σ uncertainty. Line width realizations were interpolated onto a model curve that describes the line width as a function of scale height to obtain a distribution of scale heights for each line. Finally, we computed the error weighted mean of these distributions, which is shown in Figure 6. The median scale height of this distribution occurs at $-0.75R_\star$, with a 1σ lower limit of $-0.98R_\star$, and 1σ and 3σ upper limits of $-0.46R_\star$ and $0.07R_\star$, respectively. Physically, this corresponds to the case in which emission is concentrated toward the stellar poles. The median scale height maps to a stellar surface latitude of 75° for very compact emission with respect to the stellar radius, while the 1σ limit corresponds to 57° (the 3σ upper limit allows very compact emission over the whole of the stellar surface).

3.4. Fast Fourier Transform (FFT) Analysis

The general idea behind using FFTs to probe line broadening is to use the combined signal in the whole of the spectrum, rather than just a small handful of bright, well-measured lines. Also crucial to the analysis of individual line widths is accurate knowledge of the strength and location blends that might significantly affect the observed line widths. The analysis above was based on single well-exposed lines for which blend contributions can be estimated reasonably well, provided the temperature structure and chemical composition of the corona are well understood. However, for other lines somewhat weaker than our sample the blend contributions become more significant and resulting systematic uncertainties in measured line widths commensurately larger.

In a Fourier approach, it is the distribution of power that matters and the exact placement of the myriad of weaker lines is less important. Similar Fourier techniques have been applied to high resolution optical spectra of stars, as pioneered by D. Gray et al. (e.g., Smith & Gray 1976), are also, in principle, capable of separating rotational broadening from other broadening mechanisms such as turbulence with Gaussian velocity distributions. However, *Chandra* grating spectra cover a decade in resolving power from short to longer wavelengths and the broadening signatures we seek amount to, at maximum, only a fraction of the instrumental width and such fine differentiation will not be possible.

Our method is to compare the power spectra of the observed AB Dor HETG spectra with those of synthetic spectra that have been broadened by different rotation velocities. Synthetic spectra were computed using a similar approach to that described above for individual spectral lines, using the emission measure distribution with temperature, $\Phi(T)$, in addition to element abundances, of García-Alvarez et al. (2005). Owing to the mass dependency of thermal broadening, this needs to be accounted for separately for the different elements prior to convolution with the rotational broadening function and instrumental profile.

Since a given rotational broadening contributes more to an observed line width at longer wavelengths where the instrumental resolving power is highest, power spectra generated from synthetic spectra are fairly sensitive to the relative intensities of the strongest lines across the wavelength range. While our simulated AB Dor spectra matched the observations very well in general (see, e.g., García-Alvarez et al. 2005), some of the intensities of stronger Fe lines, in particular, differed by ~30% or so from those observed. These problems are largely attributable to difficulties and complexities in theoretical predictions of the relative line strengths themselves —a problem discussed at length in the case of Fe XVII in recent work of Doron & Behar (2002) and Gu (2003). We therefore adjusted the simulated intensities of the strongest lines to match the observed intensities.

Uncertainties resulting from Poisson counting statistics were estimated for the FFT of the observed AB Dor spectrum using a

Table 2
Observed and Model Line Widths for AB Dor and μ Vel

Grating	Rest Wvl (Å)	FWHM (Å)				AB Dor Excess Relative to μ Vel[b]
		Observation		Model[a]		
		AB Dor	μ Vel	AB Dor	μ Vel	
MEG	12.13	0.021 ± 0.001	0.020 ± 0.001	0.023	0.020	−0.001
MEG	14.20	0.021 ± 0.002	0.019 ± 0.002	0.023	0.020	−0.001
MEG	15.01	0.021 ± 0.001	0.018 ± 0.001	0.022	0.019	−0.000
MEG	16.01	0.022 ± 0.002	0.017 ± 0.003	0.024	0.021	0.002
MEG	16.78	0.022 ± 0.002	0.015 ± 0.001	0.023	0.020	0.005
MEG	18.97	0.024 ± 0.001	0.019 ± 0.003	0.026	0.024	0.002
MEG	24.78	0.027 ± 0.007	0.012 ± 0.006	0.029	0.026	0.011
HEG	12.13	0.014 ± 0.001	0.015 ± 0.002	0.015	0.013	−0.003
HEG	15.01	0.011 ± 0.002	0.012 ± 0.003	0.013	0.011	−0.003

[a] Model line widths include instrumental, thermal, and surface rotational broadening.
[b] Excess line widths refer to $(w_{obs} - w_{mod})_{AB\ Dor} - (w_{obs} - w_{mod})_{\mu\ Vel}$, where w_{obs} and w_{mod} refer to observed and model line widths, respectively.

Monte Carlo method. We constructed 100 realizations of the observed spectrum by randomizing the counts in each spectral bin within their observed Poisson errors. An FFT was then computed for each of the 100 realizations, and the 1σ confidence limits on the mean FFT of the observed counts spectrum were obtained from the resulting FFT distributions. In order to facilitate comparison between FFTs of model and observed spectra, the FFTs were summed over intervals of 10 bins, where the bin size was 0.005 Å.

The observed power spectrum and uncertainties are compared with those of the synthetic spectra in Figure 7. This analysis indicates that spectra with only instrumental broadening are not a good match to the observations, and some additional broadening is required. The FFT of the model spectrum with thermal broadening and very small additional rotational broadening corresponding to a very small scale height of $0.1R_\star$ (essentially equivalent to the case of no rotational broadening) provides the best match to the observations, although models with slightly larger scale heights—up to $\leqslant 1R_\star$ or so cannot be excluded. The model corresponding to surface rotation scale height $1R_\star$ exceeds the 3σ error bounds at scales corresponding approximately to the line FWHM. This indicates that the model line core is broader than observations indicate. Models with scale heights $>1R_\star$ are strongly excluded.

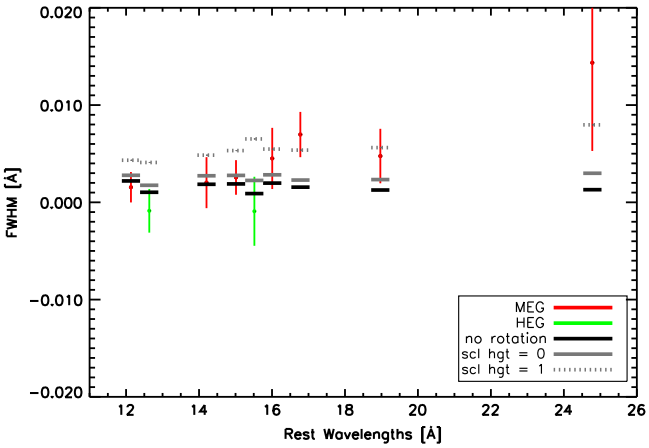

Figure 5. Illustration of the observed line widths and 1σ uncertainties of emission lines measured from the MEG and HEG spectrum of AB Dor, with the corresponding μ Vel line widths subtracted. The horizontal lines represent the model line widths of AB Dor, relative to μ Vel. The solid black horizontal line indicates predicted line widths based on a realistic, optically thin model, without rotational broadening. The solid gray and dotted gray horizontal lines represent the predicted line widths for surface rotational broadening and rotational broadening at a scale height of $1R_\star$ above the stellar surface, respectively.

4. DISCUSSION

4.1. Summary and Interpretation of Results

A careful analysis of *Chandra* HETG spectra using cross-correlation and FFT techniques has provided quantitative constraints on the coronal scale height and structure of the rapidly rotating corona on AB Dor. This information is encoded in the observed spectrum through Doppler shifts of the source plasma. These Doppler shifts amount to only a fraction of the instrumental broadening and are not easily or reliably detected in single line profiles or centroids. However, the emphasis of the study presented here is that the cross-correlation and FFT techniques we have exploited use the signal in the whole of the observed spectrum and can be more sensitive than analyses based on single lines.

Measured wavelengths of individual spectral lines illustrated in Figure 3 show no obvious or significant Doppler shifts relative to the mean frame of rest, although there is a hint of a redshift at phase $\phi = 0.9$ in lines of Mg XII λ8.42 and Fe XVII λ16.78 that is also perhaps present in O VIII λ18.97. The phase $\phi = 0.9$ corresponds exactly to the peak of the flare evident in the light curve in Figure 2 and it is tempting to ascribe the weak velocity shift signature to it. If so, it would imply the flare were situated on the receding hemisphere of AB Dor. We noted in Section 3 that it is possible that the impulsive phase of the flare was obscured by the stellar disk. Were this the case though we might have expected to see a blueshift rather than redshift, as the flare approached along the line of sight around the limb, and the lack of any net blueshift at this phase tends to argue against such an explanation. One might also expect to see blueshifted plasma as a result of chromospheric evaporation within flaring loops on the visible hemisphere in which loops are likely to be at least partly aligned along the line of sight (although to our knowledge no convincing blueshifts due to chromospheric evaporation have been detected by *Chandra* to date). That the redshift is not seen in the brighter Fe XVII λ15.01 line, however, suggests the redshift hint most prominent in

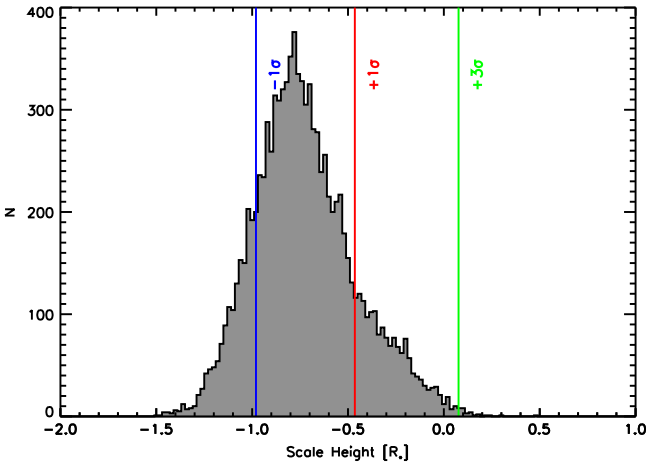

Figure 6. The error weighted mean distribution of scale heights based on a Monte Carlo analysis of observed and predicted line widths of the MEG and HEG data, as described in the text. Scale heights are relative to the stellar surface and assume spherical symmetry, such that a height of zero corresponds to a uniform corona on the stellar surface with negligible vertical extension. Negative scale heights imply the corona is restricted to high latitudes. The 1σ lower limit, along with the 1σ and 3σ upper limits are indicated by vertical lines.

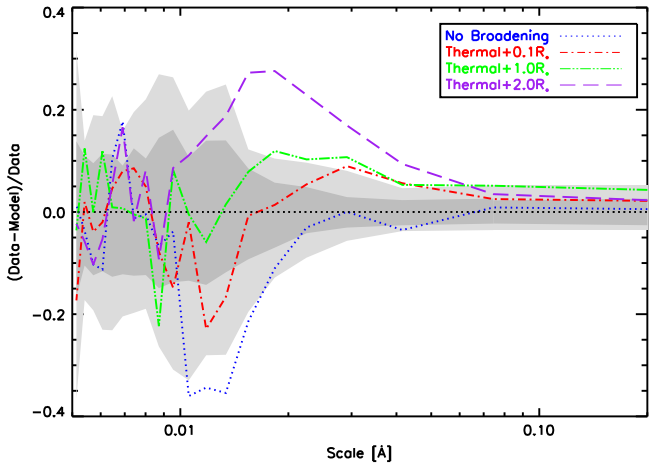

Figure 7. Comparison between fast Fourier transforms of model and observed spectra in the spectral scale size region of interest. Model spectra were computed as described in the text and were convolved with a rotational broadening function with different scale heights. Here, the scale heights refer to the radius assumed in the rotational broadening function, rather than to the additional height above surface rotation as in the preceding figure and in the text (e.g., Thermal+0.1$R_\star$ implies a rotational broadening component corresponding to a scale height of $-0.9R_\star$). The shaded regions indicate the $\pm1\sigma$ and $\pm3\sigma$ uncertainty bounds of the data obtained through Monte Carlo simulations.

Fe XVII λ16.78 is spurious with an origin in some degree of systematic uncertainty not accounted for in the analysis.

The cross-correlation of phase-resolved spectra provides a much more sensitive measure of Doppler shifts than any of the individual lines (Figure 4). Figure 4 shows that Doppler shifts are almost exclusively within 1σ of 0 km s^{-1} and are perfectly consistent with no significant net velocity shift. The lack of net Doppler shifts larger than $\sim$20 km s^{-1} implies that either coronal plasma at low latitudes was relatively uniformly distributed in longitude, or that plasma was concentrated at the poles during the 1999 October epoch analyzed here.

We noted in Section 3.2.2 that the cross-correlation technique does not distinguish between lines formed at different characteristic temperatures. In this sense, our measurements are essentially a signal-weighted average Doppler shift. Since the longer wavelengths are also more sensitive to velocity, the weighting for the MEG spectrum is going to be more toward the H-like Ne X Lyα line and Fe XVII and O VIII features longward of this. These ions are generally formed in the temperature range 2–6 $\times$ 10^6, although the increasing emission measure toward higher temperatures (e.g., García-Alvarez et al. 2005) means that weighting will be toward the high end of this range. The HEG spectrum will be more sensitive to higher temperature features, including H- and He-like Si, Mg, and Ne. These are generally formed at temperatures of 5–15 $\times$ 10^6 K. While the cross-correlation technique might mask some subtle differences in radial velocity with temperature, the agreement of HEG and MEG results and the fact that the individual lines formed at different temperatures do not show any signs of significantly different behavior, indicates that there is no temperature schism in the structure of the AB Dor corona.

The degeneracy between a corona uniformly distributed in longitude or one concentrated at the poles indicated by the lack of significant Doppler shifts can be removed by examining spectral line widths, which we would expect to exhibit palpable broadening were the corona to be uniformly distributed about the star, or concentrated at low latitudes. The line widths, however, show no evidence for strong additional rotational broadening, in contrast to the HETG spectra of Algol presented by Chung et al. (2004). Both FFT and individual line width analyses favor only very small additional broadening above that induced by thermal velocities and the instrumental profile. The median coronal scale height from the Monte Carlo simulations of all the lines combined (Figure 6) is $h = -0.75R_\star$; i.e., less than the stellar radius as measured from the stellar center. The 1σ upper limit is $-0.46R_\star$—also less than the stellar radius. Physically, these "negative" scale heights can be interpreted in terms of the corona being restricted toward high latitude where rotational broadening is smaller. Formally, the 1σ upper limit corresponds to a corona limited to latitudes >57°. Similarly, the FFT analyses also suggest the corona lies at restricted higher latitudes.

These results provide direct spectroscopic evidence that the dominant coronal emission in a rapidly rotating active star such as AB Dor is largely associated with the dark polar spots commonly found in Doppler imaging and ZDI analyses of photospheric spectra (e.g., Vogt et al. 1999; Strassmeier 2002; Jeffers et al. 2005). The results are not, however, definitive: the 3σ upper limit to the scale height based on individual lines is $h < 0R_\star$ (surface rotation or less). A rigorous formal limit is more difficult to define for the FFT analysis, but the data suggest strongly that $h < 0R_\star$. It is also not possible to rule out some small fraction of the emission as emanating from lower latitudes. Such emission would give rise to broadened line wings, of which we see no evidence in the spectra. It is, however, possible that of the order of 10% of the emission could be in a somewhat broader spectral component.

4.2. Comparison with Other Epochs

The lack of phase-related Doppler shifts in the 1999 October spectra of AB Dor contrasts with the modulation seen by Hussain et al. (2005; see also Hussain et al. 2007) in the light of O VIII λ18.97 in the LETG observation of 2002 December,

which exhibited a to peak-to-peak velocity change of 60 km s^{-1} and betrayed low-latitude structure during that epoch. Hussain et al. (2005) also investigated constraints on the coronal scale height from both *Chandra* LETG and FUSE spectra. They found $h < 0.75R_\star$ (1σ) based on the Fe XVII 15.01 Å line in the 2002 December epoch LETG spectra. Based on FUSE observations from 1999 December and 2003 December of the forbidden lines Fe XVIII λ974 and Fe XIX λ1118, they obtained $h = 0.45 \pm 0.3R_\star$. In principle, the much higher FUSE resolution ($\lambda/\Delta\lambda \sim 20,000$) should render tighter constraints on line profiles than *Chandra* spectra; unfortunately, however, the very weak forbidden Fe lines are compromised by the presence of neighboring strong lines and line blends.

A salient point that the long FUSE observation, and the *Chandra* LETG and HETG observations, were all obtained at significantly different epochs, should be borne in mind: while particular active longitudes apparently do exist on AB Dor (Järvinen et al. 2005), details of the coronal topology would be expected to change on shorter timescales and there is no reason that particular features hinted at by one observation should be present in another. Our observations indicate that the bulk of the coronal emission persists at high latitudes. Both the Doppler shifts and photometric rotational modulation found by Hussain et al. (2005) suggest that some detectable emission can also occur at lower latitudes. This picture is supported by the pattern of ambiguous EUV-X-ray rotational modulation evidence discussed in Section 2: while some observations found significant rotational modulation, others, including the extensive study of Lalitha & Schmitt (2013), did not.

Further clues as to the temporal variation of the coronal emission of AB Dor can be gleaned from Doppler and ZDI maps obtained in different years. Donati et al. (2003) presented both spot (Doppler imaging) and magnetic field (ZDI) maps for AB Dor for epochs spanning 1998-2002. All epochs exhibited an extensive dark polar spot covering latitudes above 70° or so (see also Jeffers et al. 2007), consistent with our inference of the location of the bulk of the coronal emission, and all showed some degree of structure at lower latitudes. However, qualitatively, there is quite a striking difference between maps presented for epoch 1999.97, which is fairly close to the epoch of our 1999 October observations and those presented for 2001.99 in the sense that the latter contain much more extensive features and structure at mid and low latitudes. Such structure is almost absent in the 1999.97 maps, even considering the more limited phase coverage of those observations. This matches expectations from the 1999 and 2002 *Chandra* Doppler shift results reported here and by Hussain et al. (2005), respectively. The late 1990s also corresponds to the peak in brightness—and presumably the minimum in spot coverage—of AB Dor based on the photometric monitoring of Järvinen et al. (2005).

4.3. Implications for Coronal Magnetic Field Extrapolation and Models

As noted in Section 1, the type of spectroscopic constraints on the topography of coronal plasma reported here represent potentially important observational tests of coronal structure extrapolated from ZDI maps of the photospheric magnetic field. Our deduction of predominately polar coronal activity on AB Dor is in qualitative agreement with the ubiquitous presence of extensive polar spots on AB Dor and with such coronal field extrapolation by Jardine et al. (2002a, 2002b), and Hussain et al. (2002). These authors inferred that although the corona might be quite extended, much of the model emission comes from high-latitude regions close to the stellar surface. It has been especially noted by McIvor et al. (2003), however, that ZDI cannot reveal the nature of the magnetic field in polar regions and whether field structures are predominantly closed or open. These authors have investigated the influence of different magnetic configurations on global coronal structure, while Mackay et al. (2004) have performed magnetic flux transport simulations to study the formation of polar spots. Both Coriolis forces (Schuessler & Solanki 1992) and poleward meridional flows (Schrijver & Title 2001) might contribute to the accumulation of polar fields. The latter would tend to produce concentric rings of alternating polarity, while the former might be expected to produce a mixed polarity pole. Mackay et al. (2004) find that both are actually needed to produce mixed polarity regions. Images from ZDI support the idea of a mixed polarity polar cap as the high-latitude flux that will "feed" the cap invariably consists of intermingled positive and negative field. In the models of McIvor et al. (2003), the Coriolis force and poleward meridional flow both produce coronae with dominant polar regions of closed field—regions that would be bright in X-rays and consistent with our spectroscopic constraints. Alternative models constructed by adding dipolar and unipolar field regions instead produce X-ray dark open field regions at the poles and more equatorially distributed coronae that are inconsistent with the spectroscopic evidence. Such models also imply rotational modulation in excess of observations (Jardine et al. 2002a; McIvor et al. 2003) and would also produce rotationally broadened line profiles well in excess of our observed widths.

The coronal models reconstructed by Hussain et al. (2007) based on ZDI contemporaneous with the LETG observations analyzed by Hussain et al. (2005) had a significant high-latitude component, similar to what we find here, but also some structure at low latitudes, in qualitative agreement with the LETG spectra and X-ray light curve, and with what might be expected based on the surface imaging maps. Hussain et al. (2007) noted that the potential field reconstructions of the coronal magnetic field depended on what was assumed for the surface magnetic field on the unseen pole (pointed away from the line of sight). They discussed two approaches involving mapping the field on the visible pole to the invisible one, either reversing the sign of the field in the process or not. The former produced much more rotational modulation of X-ray emission —and more than has been observed—than the latter, which was therefore preferred.

Cohen et al. (2010) have demonstrated that potential field extrapolation models for AB Dor can be quite different to self-consistent models including the stellar wind and effects of rotation. The wind acts to open up field lines that would otherwise remain closed without the additional wind forcing. Rotational drag on the field was found to wind coronal structures quite tightly around the star, even below the Alfvén radius quite close to the stellar surface. Another latent issue for coronal models of all types for active, rapid rotators based on magnetic maps was discussed in detail Arzoumanian et al. (2011), who considered the effects of dark spots on ZDI. Since this method is sensitive mainly to the magnetic field in the bright regions of the stellar surface, the magnetic signatures of the dark spots can be censored to some degree. Arzoumanian et al. (2011) modeled the magnetic field that might have been

contained in these spots on AB Dor and the similarly fast spinning, but fully convective and lesser spotted, M4 dwarf V374 Peg by adding magnetic flux to the magnetograms. The effect of missing flux for the latter star was fairly small, but very significant for AB Dor that hosts a large, seemingly permanent, polar spot. Adding polar flux of a single polarity significantly increased the model plasma emission measure as well as the rotational modulation, the latter well beyond observed limits. The correlation between X-ray luminosity and large-scale magnetic flux assessed using ZDI presented by Vidotto et al. (2014), covering several orders of magnitude in both quantities, suggests that the loss of emission measure leading to X-ray emission is probably not catastrophic and perhaps also provides some support for mixed, rather than single, polarity polar fields.

The spectroscopic study presented here again tends to support a more mixed polarity field at high latitudes, which should diminish the effects of any clumpy, azimuthally non-uniform emission at lower latitudes. The results could also be important for understanding angular momentum loss on young, rapid rotators. The presence of missed polarity in the dark polar spots will act to close down field lines there that would otherwise be expected to present a strong source of wind-driven mass loss. Alternatively, the polar regions could be a copious source of flares and coronal mass ejections (CMEs) that might dominate the mass loss of very active stars (e.g., Drake et al. 2013). The effect of the latter on angular momentum loss will be difficult to assess without greater understanding of such CME events, their opening angle, and at what distance from the star they become super-Alvénic.

The Arzoumanian et al. (2011) study presents a case for caution in interpretation of observed magnetograms for use in coronal models due to the inherent limitations of the observational technique. In addition to dark spot field censoring, limited spatial resolution can also give rise to missing flux of mixed polarity on scales similar to, or smaller than, the resolution limit. This missing flux and smearing of surface magnetic field structure can also give rise to significantly different predictions of coronal structure and emission (Johnstone et al. 2010; Garraffo et al. 2013). Spectroscopic studies such as that presented here, together with diagnostics of coronal plasma density and optical depth, are able to provide valuable observational leverage to overcome these difficulties and potent tests of the properties of coronal models.

5. CONCLUSIONS

We have demonstrated that *Chandra* HETG spectra are sufficiently sensitive to provide Doppler shift constraints on the coronal structure of AB Dor. Based on a fine analysis of individual spectral lines, and on cross-correlation and Fourier techniques, we draw the following conclusions.

1. In contrast to the finding of X-ray photometric rotational modulation and rotation-driven Doppler shifts in the light of the H-like O VIII Lyα resonance line based on LETG observations obtained in 2002 December by Hussain et al. (2005), we see no significant rotational modulation or Doppler signatures in the 1999 October spectra analyzed here. A cross-correlation analysis of both HEG and MEG spectra places stringent limits on phase-related Doppler shifts of $<20\,\mathrm{km\,s^{-1}}$. These results are qualitatively consistent with surface images that appear to show less low-latitude structure in 1999, and with observations of variable degrees of low-latitude spot coverage at different epochs (Jeffers et al. 2007). There is no evidence in the spectra for significant blueshifts associated with a modest flare that occurred toward the middle of the observation, which might be expected from chromospheric evaporation in loops aligned along the line of sight.
2. Some individual spectral lines exhibit Doppler shifts that appear to be statistically significant, but that are not seen in other spectral lines; uncertainties in observed line positions therefore contain an additional element of uncertainty above that of the formal statistics of profile fitting. As also noted by Chung et al. (2004), such additional uncertainties are likely to be associated with the stability and ultimate precision of the *Chandra* optical system.
3. Individual line widths together with Fourier analysis of the whole spectrum are consistent with model profiles with very little additional rotational broadening, indicating that the emission originates at the stellar poles. These results then provide the direct spectroscopic evidence that the dominant coronal activity on rapidly rotating active stars is associated with the dark polar spots commonly seen in photospheric Doppler images. The lack of significant rotational broadening in coronal lines support models in which these spots are of mixed magnetic polarity and able to sustain closed coronal loops, rather than of dipolar or unipolar origin.

The sensitive analysis techniques developed by Chung et al. (2004) for Algol and furthered here for AB Dor provide powerful means for investigating coronal structure of nearby rapidly rotating stars.

We thank an anonymous referee for a very helpful report that enabled us to significantly improve the manuscript. We thank the NASA AISRP for providing financial assistance for the development of the PINTofALE package and the CHIANTI project for making publicly available the results of their substantial effort in assembling atomic data useful for coronal plasma analysis. J.J.D. and V.L.K. were supported by NASA contract NAS8-03060 to the *Chandra X-ray Center* during the course of this research. DG was supported by *Chandra* grants GO1-2021, GO2-3010X, and AR4-5002X.

REFERENCES

Ake, T. B., Dupree, A. K., Young, P. R., et al. 2000, ApJL, 538, L87
Arzoumanian, D., Jardine, M., Donati, J.-F., Morin, J., & Johnstone, C. 2011, MNRAS, 410, 2472
Ayres, T. R., Brown, A., Osten, R. A., et al. 2001, ApJ, 549, 554
Barenfeld, S. A., Bubar, E. J., Mamajek, E. E., & Young, P. A. 2013, ApJ, 766, 6
Brandt, J. C., Heap, S. R., Walter, F. M., et al. 2001, AJ, 121, 2173
Brickhouse, N. S., Dupree, A. K., & Young, P. R. 2001, ApJL, 562, L75
Brinkman, A. C., Behar, E., Güdel, M., et al. 2001, A&A, 365, L324
Budding, E., Erdem, A., Innis, J. L., Oláh, K., & Slee, O. B. 2009, AN, 330, 358
Chung, S. M., Drake, J. J., Kashyap, V. L., Lin, L., & Ratzlaff, P. W. 2004, ApJ, 606, 1184
Cohen, O., Drake, J. J., Kashyap, V. L., Sokolov, I. V., & Gombosi, T. I. 2010, ApJL, 723, L64
Collier Cameron, A., Bedford, D. K., Rucinski, S. M., Vilhu, O., & White, N. E. 1988, MNRAS, 231, 131

Collier Cameron, A., Duncan, D. K., Ehrenfreund, P., et al. 1990, MNRAS, 247, 415
Collier Cameron, A., & Foing, B. H. 1997, Obs, 117, 218
Collier Cameron, A., & Robinson, R. D. 1989, MNRAS, 238, 657
Collier Cameron, A., & Woods, J. A. 1992, MNRAS, 258, 360
da Silva, L., Torres, C. A. O., de La Reza, R., et al. 2009, A&A, 508, 833
de Medeiros, J. R., & Mayor, M. 1995, A&A, 302, 745
Donati, J.-F., & Collier Cameron, A. 1997, MNRAS, 291, 1
Donati, J.-F., Collier Cameron, A., Hussain, G. A. J., & Semel, M. 1999, MNRAS, 302, 437
Donati, J.-F., Collier Cameron, A., & Petit, P. 2003, MNRAS, 345, 1187
Donati, J.-F., & Landstreet, J. D. 2009, ARA&A, 47, 333
Doron, R., & Behar, E. 2002, ApJ, 574, 518
Drake, J. J. 2003, ApJ, 594, 496
Drake, J. 2004, ChNew, 11, 8
Drake, J. J., Brickhouse, N. S., Kashyap, V., et al. 2001, ApJL, 548, L81
Drake, J. J., Chung, S. M., Kashyap, V., et al. 2008, ApJ, 679, 1522
Drake, J. J., Cohen, O., Yashiro, S., & Gopalswamy, N. 2013, ApJ, 764, 170
Dupree, A. K., Ake, T. B., Brickhouse, N. S., Hussain, G. A. J., & Jardine, M. 2006, in ASP Conf. Ser. 348, Astrophysics in the Far Ultraviolet: Five Years of Discovery with FUSE, ed. G. Sonneborn, H. W. Moos, & B.-G. Andersson (San Francisco, CA: ASP), 168
García-Alvarez, D., Drake, J. J., Ball, B., Lin, L., & Kashyap, V. L. 2006, ApJ, 638, 1028
García-Alvarez, D., Drake, J. J., Lin, L., Kashyap, V. L., & Ball, B. 2005, ApJ, 621, 1009
Garraffo, C., Cohen, O., Drake, J. J., & Downs, C. 2013, ApJ, 764, 32
Gray, D. F. 1992, The Observation and Analysis of Stellar Photospheres (2nd ed.; Cambridge: Cambridge Univ. Press)
Gu, M. F. 2003, ApJ, 582, 1241
Guirado, J. C., Marcaide, J. M., & Martí-Vidal, I. 2011, A&A, 533, A106
Guirado, J. C., Reynolds, J. E., Lestrade, J.-F., et al. 1997, ApJ, 490, 835
Guirado, J. C., Martí-Vidal, I., Marcaide, J. M., et al. 2010, in Highlights of Spanish Astrophysics V, ed. J. M. Diego, L. J. Goicoechea, J. I. González-Serrano, & J. Gorgas (Berlin: Springer), 139
Huenemoerder, D. P., Testa, P., & Buzasi, D. L. 2006, ApJ, 650, 1119
Hussain, G. A. J., Brickhouse, N. S., Dupree, A. K., et al. 2012, MNRAS, 423, 493
Hussain, G. A. J., van Ballegooijen, A. A., Jardine, M., & Collier Cameron, A. 2002, ApJ, 575, 1078
Hussain, G. A. J., Brickhouse, N. S., Dupree, A. K., et al. 2005, ApJ, 621, 999
Hussain, G. A. J., Jardine, M., Donati, J.-K., et al. 2007, MNRAS, 377, 1488
Innis, J. L., Coates, D. W., Thompson, K., & Robinson, R. D. 1985, PASAu, 6, 156
Innis, J. L., Thompson, K., Coates, D. W., & Evans, T. L. 1988, MNRAS, 235, 1411
Ishibashi, K., Dewey, D., Huenemoerder, D. P., & Testa, P. 2006, ApJL, 644, L117
Janson, M., Brandner, W., Lenzen, R., et al. 2007, A&A, 462, 615
Jardine, M., Collier Cameron, A., & Donati, J.-F. 2002a, MNRAS, 333, 339
Jardine, M., Wood, K., Collier Cameron, A., Donati, J.-F., & Mackay, D. H. 2002b, MNRAS, 336, 1364
Järvinen, S. P., Berdyugina, S. V., Tuominen, I., Cutispoto, G., & Bos, M. 2005, A&A, 432, 657
Jeffers, S. V., Collier Cameron, A., Barnes, J. R., Aufdenberg, J. P., & Hussain, G. A. J. 2005, ApJ, 621, 425
Jeffers, S. V., Donati, J.-F., & Collier Cameron, A. 2007, MNRAS, 375, 567
Johnstone, C., Jardine, M., & Mackay, D. H. 2010, MNRAS, 404, 101
Kashyap, V., & Drake, J. J. 2000, BASI, 28, 475
Kuerster, M., Schmitt, J. H. M. M., Cutispoto, G., & Dennerl, K. 1997, A&A, 320, 831
Lalitha, S., Fuhrmeister, B., Wolter, U., et al. 2013, A&A, 560, A69
Lalitha, S., & Schmitt, J. H. M. M. 2013, A&A, 559, A119
Luhman, K. L., Stauffer, J. R., & Mamajek, E. E. 2005, ApJL, 628, L69
Mackay, D. H., Jardine, M., Cameron, A. C., Donati, J.-F., & Hussain, G. A. J. 2004, MNRAS, 354, 737
Maggio, A., Pallavicini, R., Reale, F., & Tagliaferri, G. 2000, A&A, 356, 627
McCarthy, K., & Wilhelm, R. J. 2014, AJ, 148, 70
McIvor, T., Jardine, M., Cameron, A. C., Wood, K., & Donati, J.-F. 2003, MNRAS, 345, 601
Ness, J.-U., Güdel, M., Schmitt, J. H. M. M., Audard, M., & Telleschi, A. 2004, A&A, 427, 667
Pakull, M. W. 1981, A&A, 104, 33
Robinson, R. D., & Collier Cameron, A. 1986, PASAu, 6, 308
Rucinski, S. M. 1985, MNRAS, 215, 615
Sanz-Forcada, J., Brickhouse, N. S., & Dupree, A. K. 2003a, ApJS, 145, 147
Sanz-Forcada, J., Maggio, A., & Micela, G. 2003b, A&A, 408, 1087
Schmitt, J. H. M. M., Krautter, J., Appenzeller, I., et al. 1997, A&A, 325, 249
Schrijver, C. J., & Title, A. M. 2001, ApJ, 551, 1099
Schuessler, M., & Solanki, S. K. 1992, A&A, 264, L13
Smith, M. A., & Gray, D. F. 1976, PASP, 88, 809
Strassmeier, K. G. 2002, AN, 323, 309
Testa, P., Drake, J. J., & Peres, G. 2004a, ApJ, 617, 508
Testa, P., Drake, J. J., Peres, G., & DeLuca, E. E. 2004b, ApJL, 609, L79
Testa, P., Drake, J. J., Peres, G., & Huenemoerder, D. P. 2007, ApJ, 665, 1349
Torres, C. A. O., Quast, G. R., Melo, C. H. F., & Sterzik, M. F. 2008, in Young Nearby Loose Associations, ed. B. Reipurth (San Francisco, CA: ASP), 757
Vidotto, A. A., Gregory, S. G., Jardine, M., et al. 2014, MNRAS, 441, 2361
Vilhu, O., Gustafsson, B., & Edvardsson, B. 1987, ApJ, 320, 850
Vilhu, O., Tsuru, T., Collier Cameron, A., et al. 1993, A&A, 278, 467
Vogt, S. S., Hatzes, A. P., Misch, A. A., & Kürster, M. 1999, ApJS, 121, 547
Walter, F. M. 2004, AN, 325, 241
White, S. M., Lim, J., Rucinski, S. M., et al. 1996, in IAU Coll. 152, Astrophysics in the Extreme Ultraviolet, ed. S. Bowyer, & R. F. Malina (Dordrecht: Kluwer Academic), 165
Wolter, U., Czesla, S., Fuhrmeister, B., et al. 2014, A&A, 570, A95
Zuckerman, B., Song, I., & Bessell, M. S. 2004, ApJL, 613, L65